ACS APPLIED POLYMER MATERIALS

pubs.acs.org/acsapm

Article

# Structural Investigation on Electrospun Nanofibers from Postconsumer Polyester Textiles and PET Bottles

Yelin Ko, Juan P. Hinestroza, and Tamer Uyar*

Cite This: ACS Appl. Polym. Mater. 2023, 5, 7298−7307

Read Online

ACCESS | Metrics & More | Article Recommendations | Supporting Information

**ABSTRACT:** This study investigates the structural and physical properties of electrospun nanofibers (NF) produced from postconsumer poly(ethylene terephthalate) (PET) textile sources, including a no-dye polyester fabric, a 50/50 (by weight) mixture of red- and blue-dye polyester fabric, a polyester t-shirt, and from a postconsumer PET bottle. The postconsumer PET sources and their corresponding electrospun NF exhibited similar chemical structures and melting points. However, the electrospun PET NF showed distinct cold crystallization and sharper melt-crystallization behavior during rapid cooling as well as improved resolution of their Fourier transform infrared spectra. We hypothesize that this behavior can be attributed to the presence of locally ordered mesophases in the electrospun PET NF caused by rapid stretching of the electrically charged jet during electrospinning. The electrospun NF were found to be more amorphous, to have a lower degree of crystallinity, and to exhibit weakened signals of the trans conformers of the glycol units, when compared to their original postconsumer PET sources. Polyester-textile NF showed smaller average fiber diameters, higher degrees of crystallinity, higher melt-crystallization temperatures, and more rigidity than those of NF produced from PET bottles. The electrospun NF acquired from postconsumer PET textiles and bottles may hold promise as a versatile material for filtration, protective clothing, and environmental remediation.

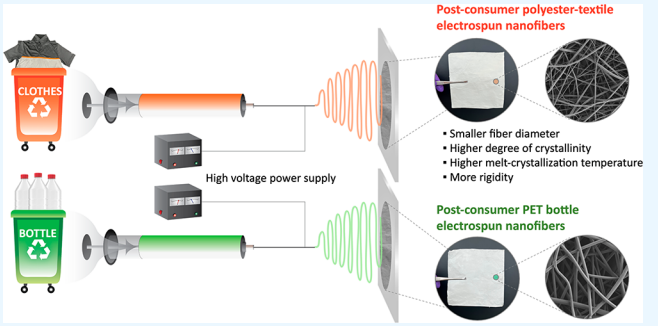


**KEYWORDS:** *electrospinning, nanofibers, polyester fabrics, recycling textiles, PET bottles, structure−property relations*



## INTRODUCTION

According to the U.S. Environmental Protection Agency, approximately 17 million tons of textiles are discarded annually in the United States.[1] However, only 15% of those discarded textiles are currently being recycled, while 66% of them end up in landfills, and 19% are incinerated.[1] Poly(ethylene terephthalate) (PET) fibers, commonly known as polyester fibers in textile applications, represent the single largest volume of fibers consumed worldwide, accounting for 50% of the global fiber market. Moreover, the consumption of polyester fibers has grown at an annual rate of 7%.[2] Although polyester fibers offer benefits to consumers such as being lightweight, durable, chemically resistant, and versatile during their lifetime use, their non-biodegradable nature poses a significant challenge in the postconsumer stage.

Electrospinning produces nanofibers (NF) and nanofibrous structures with a significantly high surface area-to-volume ratio, nanosized pores, unique physical and mechanical properties, and the potential to become functionalized surfaces.[3] A variety of commercial-scale electrospinning equipment already exists,[4] proving its amenability to large-scale production. Most published reports have focused on using PET bottles as the primary source for electrospinning. For example, Topuz et al. reported the development of electrospun NF from PET bottles and explored the use of the resulting NF in oil removal applications.[5] In another study, electrospun NF were prepared using PET bottles and used as smoke filters.[6] Song et al. proposed a strategy to control the porous morphology of electrospun NF produced from PET bottles to develop a membrane for the filtration of PM2.5 particulate material and proteins from virus.[7] Hossain et al. recently investigated the morphological, mechanical, moisture management, and filtration properties of their electrospun NF obtained from PET bottles and demonstrated the suitability of the membranes in air filtration applications.[8] Additional works have included the development of functionalized recycled PET-based membranes for oil/water separation[9] and water treatment[10] as well as acoustic adsorption and sound transmission.[11]

Regarding the use of postconsumer polyester fabrics as a source for electrospinning, Chen et al. proposed an approach for producing laminated, recycled PET-based membranes from

Received: June 9, 2023
Accepted: August 10, 2023
Published: August 22, 2023

**Scheme 1. Production of Electrospun NF Using Postconsumer Polyester Textiles and PET Bottles**

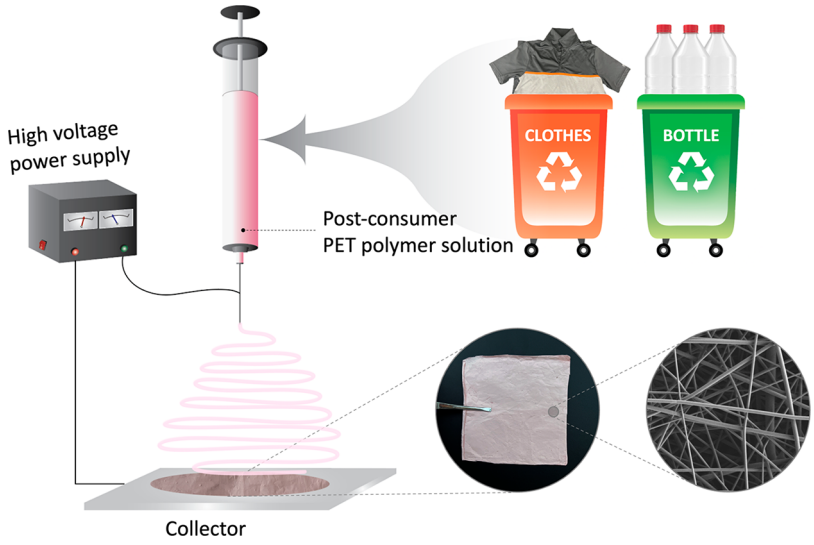


polyester fabrics for applications in sweat transportation and thermal management.[12] Although several applications of postconsumer PET NF have been reported, systematic investigations on the structural, thermal, and mechanical properties of those NF have been largely overlooked. These properties depend on the reorganization and orientation of the polymer chains during electrospinning, which occur due to high shear forces and Columbic interactions.[13] Polyester fibers are typically manufactured through melt spinning followed by drawing and heat-setting processes that enhance the fibers' crystallinity. On the other hand, PET bottles are produced via injection molding, which lacks extensive stretching and alignment. In addition, fiber-grade PET has a molecular weight ranging from 15,000 to 20,000 g·mol$^{-1}$, which is lower compared to that of bottle-grade PET, which usually lies within the range of 24,000−36,000 g·mol$^{-1}$.[14] These distinctions between PET in textiles and PET in bottles are expected to contribute to differences in the reorganization behavior of PET polymer chains when the nanofibers are formed through electrospinning.

Given the dearth of literature on electrospun NF produced from postconsumer polyester textiles, we were motivated to contribute to the field in two ways. First, we investigated the rearrangement behavior of PET chains in the NF produced from postconsumer polyester textiles, which, to the best of our knowledge, has not been previously reported. Second, we provide a comparison between the properties of the electrospun NF obtained from postconsumer polyester textiles and from PET bottles, which has not been previously studied. The structural changes as well as properties of these electrospun NF may offer valuable insights for designing NF with potential applications in filtration, protective clothing, and environmental uses. To achieve these goals, we used the following postconsumer PET objects as the polymer sources for electrospinning: undyed and dyed polyester fabrics, a polyester t-shirt, along with a PET bottle as a baseline (Scheme 1).

## EXPERIMENTAL SECTION

**Materials.** Polyester fabrics without any dyes (100% polyester knit, lot 2926), with red dye (100% polyester knit, disperse dye rust, lot 3044), and with blue dye (100% polyester knit, disperse dye blue, lot 6554) were purchased from Testfabrics, Inc. (United States). A polyester t-shirt (100% polyester) was procured from a local user, washed in a commercial washer, and dried before use. After the labels were removed, a Coca-Cola PET bottle purchased in a grocery store in the United States was cleaned, rinsed with pure ethanol, and dried. Digital photos of the original postconsumer PET sources are shown in Figure S1. Trifluoroacetic acid (TFA, Sigma-Aldrich, 99%) and dichloromethane (DCM, Sigma-Aldrich, 99.8%) used in a spinning solvent system were used as received.

**Preparation of the Electrospinning Solutions.** Four different postconsumer PET sources were used for electrospinning: (1) a no-dye polyester fabric, (2) a 50/50 (by weight) mixture of red- and blue-dye polyester fabric, (3) a 100% polyester t-shirt, and (4) a PET bottle. These polyester textiles and the PET bottle were cut into small pieces. A solvent system consisting of a 50/50 (by volume) mixture of TFA and DCM was used to dissolve the postconsumer PET sources. The PET solutions were stirred at room temperature until they became homogeneous. The polymer concentration was optimized by referring to previous studies.[15,16] Upon observing that the 20% (w/v, with respect to the solvent) polymer concentration produced NF with beaded morphology (Figure S2a), we increased the polymer concentration to 24% (w/v) to obtain uniform and bead-free NF morphology (Figure S2b).

**Electrospinning of NF from Postconsumer PET sources.** A solution from the different postconsumer PET sources was transferred into a 1 mL plastic syringe fitted with a 27 G metallic needle (inner diameter = 0.21 mm). The syringe was mounted horizontally on a syringe pump at a flow rate of 0.5 mL·h$^{-1}$. Electrospun NF were deposited onto a grounded, stationary metal collecting plate covered with aluminum foil. The tip-to-collector distance was 15 cm. A voltage of 16 kV was supplied to the needle through an alligator clip. The observed temperature during the electrospinning was ∼20 °C, while the relative humidity was ∼21%. Before any characterization, the electrospun NF were left overnight in a fume hood at room temperature to ensure the complete evaporation of the spinning solvent.

**Characterization.** Scanning electron microscopy (SEM) images of the electrospun PET NF were obtained at 2.0 kV by using a Zeiss Gemini 500 scanning electron microscope. The NF samples were fixed onto carbon tape and surrounded by a layer of silver paste, after which a thin gold−palladium coating was applied. The average fiber diameter ($D$) was calculated by using ImageJ software with 100 points and presented as a mean ± standard deviation (SD). Differential scanning calorimetry (DSC) was performed using a TA Instruments Q2000. Each sample was measured in triplicate, and the data are presented as mean ± SD. Samples with an average mass of 2.02 ± 0.01 mg were heated from 25 to 300 °C at a heating rate of 10 °C·min$^{-1}$. Following heating, the samples were held at 300 °C for 5 min



https://doi.org/10.1021/acsapm.3c01232
ACS Appl. Polym. Mater. 2023, 5, 7298−7307

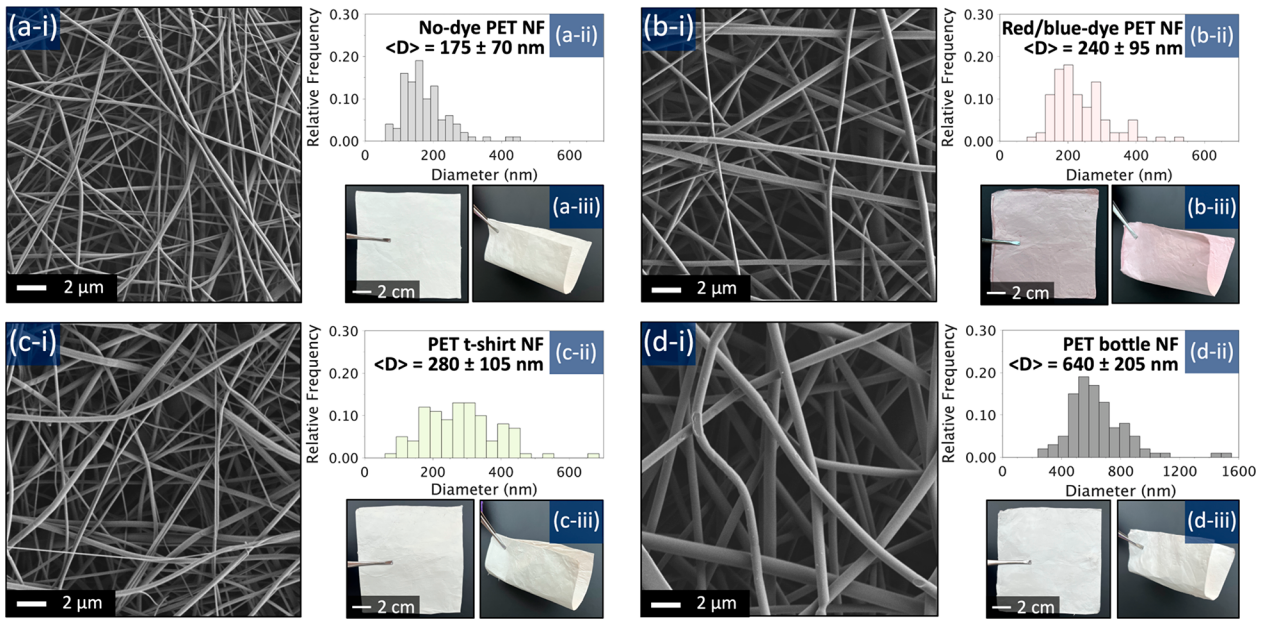


**Figure 1.** (i) SEM images, (ii) fiber diameter distributions, and (iii) digital photos of the electrospun nanofibers produced from (a) the no-dye polyester fabric, (b) the 50/50 mixture of the red- and blue-dye polyester fabric, (c) the polyester t-shirt, and (d) the PET bottle.

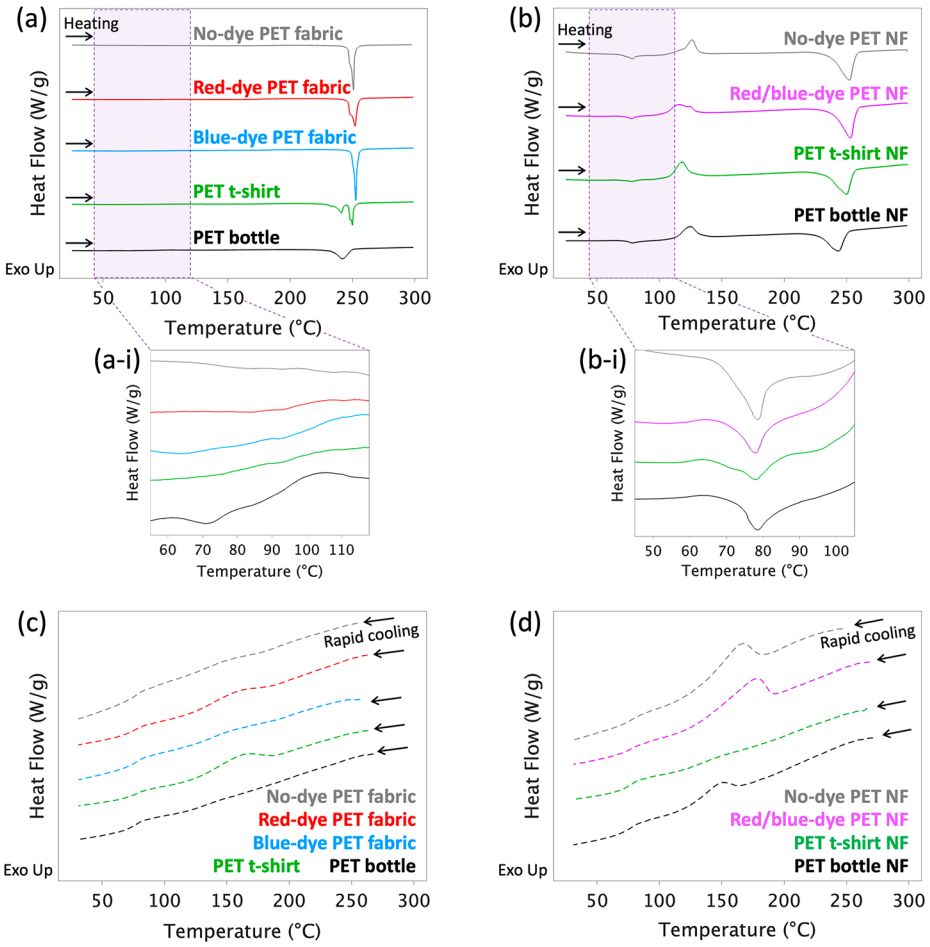


**Figure 2.** DSC curves of the original postconsumer PET sources and their corresponding electrospun NF: (a) heating scans for the no-dye polyester fabric, the red-dye polyester fabric, the blue-dye polyester fabric, the polyester t-shirt, and the PET bottle. (a–i) Heating scans for the original postconsumer PET sources near $T_g$ and $T_{cc}$. (b) Heating scans for the corresponding electrospun PET NF. (b–i) Post-$T_g$ endotherm peaks of the electrospun PET NF. (c) Cooling scans for the no-dye polyester fabric, the red-dye polyester fabric, the blue-dye polyester fabric, the polyester t-shirt, and the PET bottle. (d) Cooling scans for their corresponding electrospun PET NF.



https://doi.org/10.1021/acsapm.3c01232
ACS Appl. Polym. Mater. 2023, 5, 7298−7307

Table 1. Summary of DSC Results for the Original Postconsumer PET Sources and Their Corresponding Electrospun NF

| | $T_g$ (°C) | $T_{cc}$ (°C) | $\Delta H_{cc}$ (J/g) | $T_m$ (°C) | $\Delta H_m$ (J/g) | $T_{mc,\ rapid\ cooling}$ (°C) | $\Delta H_{mc,\ rapid\ cooling}$ (J/g) | % Crystallinity |
|---|---|---|---|---|---|---|---|---|
| Original postconsumer PET sources | | | | | | | | |
| No-dye PET fabric | Broad transition | Not clear | | 250.9 ± 0.1 | 59.5 ± 0.9 | Not clear | | 42.5 ± 0.6 |
| Red-dye PET fabric | Broad transition | Not clear | | 252.3 ± 0.3 | 60.5 ± 0.9 | 159.0 ± 0.4 | 44.5 ± 2.8 | 43.2 ± 0.7 |
| Blue-dye PET fabric | Broad transition | Not clear | | 252.8 ± 0.2 | 61.1 ± 0.4 | Not clear | | 43.6 ± 0.3 |
| PET t-shirt | Broad transition | Not clear | | 250.2 ± 0.3 | 59.1 ± 0.9 | 162.8 ± 0.5 | 77.2 ± 5.7 | 42.1 ± 0.6 |
| PET bottle | 63.7 ± 0.8 | 103.5 ± 0.9 | 5.0 ± 0.6 | 242.1 ± 0.1 | 50.6 ± 0.3 | Not clear | | 32.8 ± 0.1 |
| Electrospun PET NF | | | | | | | | |
| No-dye PET NF | 72.7 ± 1.0 | 126.7 ± 0.3 | 20.7 ± 0.6 | 252.6 ± 0.2 | 47.8 ± 0.9 | 165.7 ± 2.9 | 137.6 ± 3.3 | 19.4 ± 0.2 |
| Red/blue-dye PET NF | 72.5 ± 0.8 | 116.6 ± 0.2 | 21.9 ± 1.8 | 253.4 ± 0.1 | 49.6 ± 1.4 | 173.2 ± 3.3 | 142.6 ± 0.9 | 19.8 ± 0.3 |
| PET t-shirt NF | 73.0 ± 0.2 | 117.6 ± 1.3 | 20.1 ± 2.1 | 250.2 ± 0.1 | 48.8 ± 1.6 | Not clear | | 20.5 ± 0.6 |
| PET bottle NF | 75.1 ± 0.9 | 125.5 ± 0.3 | 21.8 ± 3.1 | 243.4 ± 0.3 | 37.5 ± 2.2 | 149.7 ± 2.7 | 65.3 ± 3.7 | 11.2 ± 0.6 |

and then rapidly cooled to 25 °C at a rate of −200 °C·min$^{-1}$. The degree of crystallinity (%crystallinity) was calculated based on the following eq 1

$$\%\text{crystallinity} = \frac{\Delta H_m - \Delta H_{cc}}{\Delta H_c} \times 100\% \quad (1)$$

where $\Delta H_m$ represents the enthalpy of melting and $\Delta H_{cc}$ is the enthalpy of cold crystallization, which is obtained from the DSC thermograms. $\Delta H_c$ represents the enthalpy of 100% crystalline polyester, which is 140.1 J/g.[17]

Fourier transform infrared (FTIR) spectra of the original postconsumer PET sources and the electrospun PET NF were collected using a PerkinElmer FTIR spectrophotometer over a range of 4000−600 cm$^{-1}$ with a 2 cm$^{-1}$ resolution. The FTIR spectra were normalized using the 1410 cm$^{-1}$ peak, which is assigned to the in-plane deformation of the benzene ring.[18] This peak is generally adopted as an internal standard because it remains unaffected by changes in molecular orientation or conformations.[19] Choosing the 1410 cm$^{-1}$ peak helps in correcting any potential variations that may arise due to sample positioning or surface defects.[20] The trans/gauche peak area ratio (T/G ratio) was calculated by using Spectrum software. X-ray diffraction (XRD) patterns of the electrospun PET NF were acquired using a Rigaku SmartLab X-ray diffractometer operating between diffraction angles of 5° to 40°, with a step size of 0.01° and a speed duration time of 1 s.

Tensile testing of the electrospun PET NF was performed using an Instron Universal Testing Machine (Instron 5566, United States) with a crosshead speed of 1 mm·min$^{-1}$ and a 100 N load cell. Specimens were cut into rectangles 10 mm wide and 40 mm long, and the two ends of each specimen were secured to the grips fixed at a gauge length of 30 mm. Three specimens were tested for each electrospun PET NF. The Young's modulus of each sample was calculated as the slope of the initial linear elastic region in the stress−strain curve. Thermogravimetric analysis (TGA) of the electrospun PET NF was conducted using a TGA analyzer (Q500, TA Instruments) by heating the samples from 25 to 700 °C in an $N_2$ atmosphere at a rate of 10 °C·min$^{-1}$. The average mass of the samples for TGA was 2.66 ± 0.04 mg.

## RESULTS AND DISCUSSION

**Morphology of Polyester-Textile NF and PET Bottle NF.** As presented in Figure 1, all of the electrospun NF samples obtained from the no-dye polyester fabric, the 50/50 mixture of red- and blue-dye polyester fabric, the polyester t-shirt, and the PET bottle formed free-standing and foldable nanofibrous webs. The average fiber diameter of the electrospun nanofibrous samples was calculated as 175 ± 70 nm for the no-dye PET NF, 240 ± 95 nm for the 50/50 mixture of red- and blue-dye PET NF, 280 ± 105 nm for the PET t-shirt NF, and 640 ± 205 nm for the PET bottle NF (Figure 1ii). The smaller average fiber diameters observed in the electrospun NF produced from the polyester textile sources suggest a higher degree of fiber stretching[21] during electrospinning in comparison to the PET bottle NF. This finding will be further discussed below.

**Crystallization and Melting Behavior of Polyester-Textile NF and PET Bottle NF.** Figure 2 presents the heating and rapid-cooling thermograms for the postconsumer PET sources as well as their corresponding electrospun NF. Table 1 shows the glass transition temperature ($T_g$), the cold crystallization temperature ($T_{cc}$), $\Delta H_{cc}$, the melting temperature ($T_m$), $\Delta H_m$, the melt-crystallization temperature during rapid cooling ($T_{mc,\ rapid\ cooling}$), the enthalpy of melt-crystallization during rapid cooling ($\Delta H_{mc,\ rapid\ cooling}$), and % crystallinity. Compared to the PET bottle, the original polyester textile sources exhibited higher %crystallinity (Table 1). Additionally, the polyester textiles showed a broad glass transition and unclear cold crystallization, whereas the PET bottle showed relatively distinct behavior (Figure 2a−i and Table 1). This difference can be attributed to the heat-setting and drawing process involved in the production of polyester textile fibers, which increases the amount of crystallinity.[22] Similar unclear glass transition and cold crystallization behavior have commonly been observed for annealed PET samples.[23,24] The growth of the crystalline region restricts the mobility of the chains in the amorphous phase, leading to a broadening of the glass transition range.[25] Cold crystallization arises from the presence of highly ordered chains that can easily reorganize into crystals.[26] Therefore, it is likely that those locally aligned chains transformed into crystals during the heat-setting process of polyester textile manufacturing. To further support the above discussion, Figure S3 shows the DSC thermogram of the PET t-shirt NF subjected to a 1-h heat setting at 150 °C, along with that of the as-spun PET t-shirt NF. The prominent $T_g$ and $T_{cc}$ observed in the as-spun NF were no longer evident in the heat-set PET t-shirt NF. This observation is consistent with previous reports[25,26] and provides evidence of how heat-setting could have affected the polymer chains of the polyester textile fibers.

The $T_m$ values before and after electrospinning the postconsumer PET sources showed no significant change, which is in agreement with previous literature.[27] The polyester textile sources and their corresponding electrospun NF exhibited $T_m$ values ranging from 250 to 253 °C (Table 1). The PET bottle and its corresponding NF showed a $T_m$ range of 242−243 °C (Table 1). These data corroborate the values reported in previous studies.[6,7,28,29] Compared to the original postconsumer PET sources, the corresponding electrospun



https://doi.org/10.1021/acsapm.3c01232
ACS Appl. Polym. Mater. 2023, 5, 7298−7307

PET NF showed significantly lower %crystallinity (Table 1) and exhibited distinct glass transitions as well as cold crystallization behavior (Figure 2a,b). The decreased % crystallinity in the PET NF is attributed to the rapid evaporation of the highly volatile solvent system (TFA/DCM) during the electrospinning process. Stretched chains lack sufficient time to arrange themselves into well-defined crystal structures before solidification occurs.[30] Instead, locally aligned but rotationally disordered chains in the noncrystalline region[31] are produced by the electrohydrodynamic forces during electrospinning.[32] This phase is referred to as a mesophase,[31,33] and its formation can explain the more defined cold crystallization observed in the electrospun PET NF (Figure 2b).

The formation of increased order and chain packing in the noncrystalline region has also been documented by Joijode et al.[34] The authors investigated three different PET samples: the as-received PET (asr-PET), PET precipitated by TFA and acetone (p-PET), and self-nucleated PET film (nuc-PET) obtained by introducing 5% p-PET as a nucleating agent to asr-PET. The density of the noncrystalline region in nuc-PET was notably higher than that of asr-PET, even though both PETs showed the same %crystallinity. This difference was ascribed to the presence of extended as well as less randomly coiled polymer chains in the noncrystalline region of nuc-PET. Comparatively, while %crystallinity decreases due to electrospinning, the polymer chains may reorganize and form enhanced order in the noncrystalline region of the NF. When heated above $T_g$, the oriented and extended polymer chains in the noncrystalline regions become mobile and serve as raw nuclei, initiating the chain-folding process and leading to crystal growth.[32] As shown in Figure 2b−i, post-$T_g$ endotherm peaks were observed in the electrospun NF, which were attributed to the partial melting of the mesophase according to several reports.[32,35] Based on previous literature, the movement of the disordered chains, which appears above $T_g$, can disrupt the nearby locally ordered chains, resulting in the emergence of a small endothermic peak after $T_g$.[36]

The electrospun NF produced from the polyester textile sources and the PET bottle showed significant differences in their %crystallinity. As shown in Table 1, the no-dye PET NF, the 50/50 mixture of red- and blue-dye PET NF, and the PET t-shirt NF exhibited crystallinity of 20%, whereas the PET bottle NF exhibited a crystallinity level of 11%. According to Zuo et al., stretching at high temperatures leads to the disentanglement of polymer chains,[37] which is also likely to occur during the fiber drawing process for polyester textile fibers. Fewer chain entanglements in a polymer solution are associated with increased chain extensibility and enhanced chain molecular orientation, as well as the production of smaller fiber diameters.[38−40] The electrospun NF produced from the polyester textile sources exhibited smaller average fiber diameters compared to that of the PET bottle NF (Figure 1ii). However, it should be noted that increased chain molecular orientation in finer electrospun nanofibers does not necessarily correspond to an increase in %crystallinity, as reported in previous studies.[38,41,42] Some studies have reported that %crystallinity decreased as the fiber diameter decreased and the chain alignment improved,[38] whereas others have suggested that %crystallinity could increase with the enhanced chain alignment.[41,42] Confined crystallization provides an explanation for the observed increase in %crystallinity when the fiber diameter decreases. The small confinement spaces within nanofibers, along with the application of mechanical forces during electrospinning, result in the formation of tightly packed chains and facilitate the arrangement of ordered crystals.[42]

To investigate whether the higher %crystallinity observed in the polyester-textile NF, compared to that of the PET bottle NF, could be attributed to the confinement effect, we produced an additional NF sample. To reduce the fiber diameter of the PET bottle NF, which originally had the largest average diameter of 640 nm, we added 1% (w/v) (with respect to the solvent) of tetrabutylammonium chloride (TBAC) to the spinning solution. It is well-known that adding salts to polymer solutions induces stronger elongation forces by increasing the charge density in the ejected jets, hence producing thinner fibers.[43] The resulting PET solution was electrospun using the same electrospinning parameters as those employed for the other PET NF. As shown in Figure S4a,b, the TBAC-incorporated PET bottle NF showed a decreased average fiber diameter of 200 ± 40 nm. Figure S4c shows the DSC curve of the TBAC-incorporated PET bottle NF. The %crystallinity value was 20.5%, which is significantly higher than the 11% crystallinity of the PET bottle NF produced without TBAC. Based on these comparisons, we speculate that the polymer chains in the spinning solution of the polyester textile sources possessed higher extensibility during electrospinning, leading to the production of the thinner fibers while facilitating chain packing and crystal formation.

Figure 2c,d show the rapid-cooling scan of the original postconsumer PET sources and their corresponding electrospun NF. The original no-dye, red-dye, and blue-dye polyester fabrics and PET bottle exhibited no clear or negligible melt crystallization during rapid cooling (Figure 2c). However, their corresponding electrospun NF displayed distinct melt-crystallization peaks, as presented in Figure 2d. These observed distinctions in the melt-crystallization behaviors resemble those between asr-PET, p-PET, and nuc-PET reported by Joijode et al.[34] While asr-PET behaved as a slow crystallizer during cooling, p- and nuc-PETs exhibited distinct melt crystallization. These differences were attributed to the presence of extended conformations of the PET chains in the noncrystalline region, such as gauche± —O−$CH_2$—, trans —$CH_2$—$CH_2$—, and gauche∓ —$CH_2$—O—. These conformations facilitate the required rotation to trans, enabling crystallization through facile counter-rotation.

When polymer chains are subjected to a "self-nucleation temperature ($T_s$)" higher than $T_m$, three types of "$T_s$ Domains" are formed.[44] First, $T_s$ Domain I occurs when $T_s$ is high enough to induce the complete melting of crystals, where no self-nuclei or crystal fragments can persist. At intermediate $T_s$ levels, the sample undergoes almost complete melting, but residual small crystal fragments or remnants of crystal memory are still present. The residual crystalline seeds can serve as self-nuclei and facilitate melt crystallization during subsequent cooling ($T_s$ Domain II). In $T_s$ Domain III, the melting process is only partial due to too-low levels of $T_s$. The remaining crystals experience annealing during treatment at $T_s$, while the molten crystals self-nucleate during subsequent cooling. The $T_s$ value of 300 °C used in our study appears to have triggered $T_s$ Domain III for the original polyester textile samples as they showed negligible melt crystallization. Meanwhile, $T_s$ Domain II seems to have been induced for their corresponding electrospun NF. This could be attributable to the presence of predominantly unentangled, extended chain conformations


https://doi.org/10.1021/acsapm.3c01232
ACS Appl. Polym. Mater. 2023, 5, 7298−7307

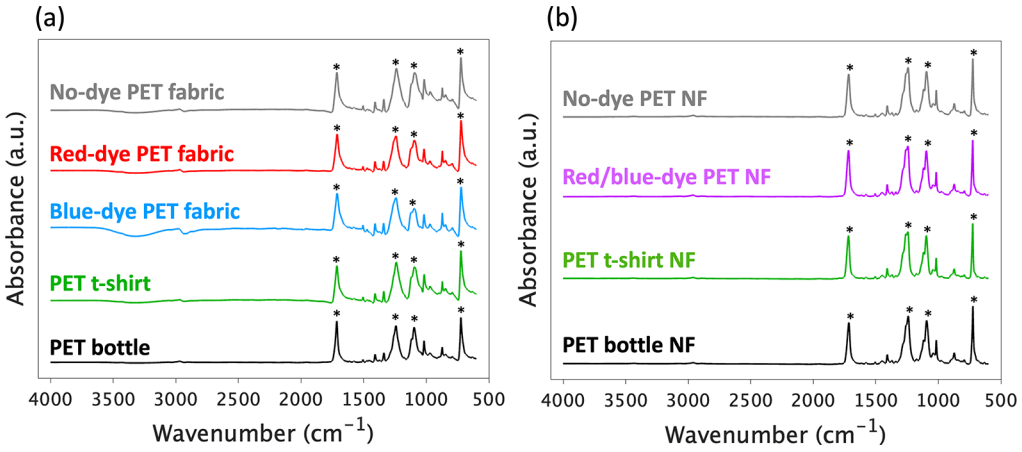


**Figure 3.** FTIR spectra of (a) the original postconsumer PET sources, including the no-dye polyester fabric, the red-dye polyester fabric, the blue-dye polyester fabric, the polyester t-shirt, and the PET bottle, and (b) their corresponding electrospun NF.

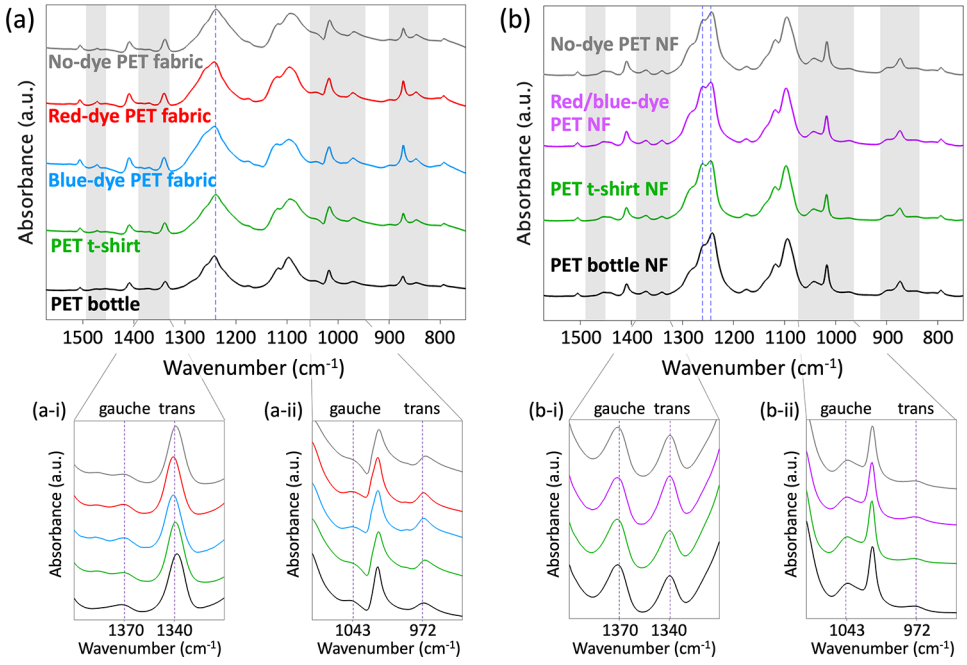


**Figure 4.** FTIR spectra in the range of 800−1500 $cm^{-1}$ for (a) the original postconsumer PET sources, including the no-dye polyester fabric, the red-dye polyester fabric, the blue-dye polyester fabric, the polyester t-shirt, and the PET bottle, and (b) their corresponding electrospun NF. The expansions of each figure represent the gauche and trans peak pairs (i) at 1370 and 1340 $cm^{-1}$ and (ii) at 1043 and 972 $cm^{-1}$.

in the noncrystalline region, which create active sites for nucleation during melt crystallization.[34] It is worth noting that the polyester t-shirt and its corresponding NF deviate from this trend. We attribute this behavior to industrial treatments applied to the polyester t-shirt fibers or the presence of additives and finishes.

As shown in Table 1 and Figure 2d, higher melt-crystallization temperatures were observed for the polyester-textile NF in comparison to the PET bottle NF. Melt crystallization at higher temperatures during the cooling process is associated with an increase in the nucleation density due to an enhanced self-nucleation process.[45] Therefore, we speculate that the melt of the polyester-textile NF contained a higher concentration of self-nuclei compared to that of the PET bottle NF. The significantly higher presence of the crystalline region in the electrospun NF produced from the polyester textile sources, supported by their higher % crystallinity, may be related to the greater survival of pristine crystals during heating. These surviving crystals are commonly associated with the origin of self-nuclei.[44]

**Chemical and Structural Properties of Polyester-Textile NF and PET Bottle NF.** The FTIR spectra of the original postconsumer PET sources and their corresponding electrospun NF are shown in Figure 3. Characteristic peaks of the innate PET structures were observed in the original postconsumer PET sources (Figure 3a) and their corresponding electrospun NF (Figure 3b). The spectra were consistent with reported literature.[6] The peaks at 1714, 1240, 1092, and 722 $cm^{-1}$ are assigned to the ester C═O group of terephthalic acid, the asymmetric stretching of the C−C−O and O−C−C groups, and the C−H wagging vibrations of the benzene ring.[6] We did not observe peaks attributed to the presence of TFA or DCM in the electrospun NF.



https://doi.org/10.1021/acsapm.3c01232
ACS Appl. Polym. Mater. 2023, 5, 7298−7307

An improved resolution of the FTIR spectra was observed in the electrospun PET NF (Figure 3b), indicated by sharper and better-defined IR bands compared to the baseline. The FTIR spectra of the original postconsumer PET sources reveal broader IR bands (Figure 3a), suggesting the presence of a diverse array of polymer conformations and chain-packing environments around each vibrating molecular bond or group.[20] To investigate the changes in chain conformations and polymer structures after electrospinning, we analyzed the FTIR spectra in the range of 800−1500 $cm^{-1}$, as presented in Figure 4. We selected this range because it includes vibrational bands that are sensitive to conformational changes.[46]

The trans−gauche peak pairs resulting from the vibrations of the glycol moiety are depicted in the expanded view of Figure 4 and Figure S5. The peaks at 1370 and 1340 $cm^{-1}$ are associated with the gauche and trans conformations resulting from the $CH_2$ wagging vibration of the glycol moiety. The peaks at 1043 and 972 $cm^{-1}$ are related to the gauche and trans conformers of the C−O stretching vibration of the glycol unit.[47] Additionally, the peaks at 898 and 848 $cm^{-1}$ represent the gauche−trans conformation pairs of the $CH_2$ rocking, and the peaks at 1453 and 1471 $cm^{-1}$ correspond to the gauche and trans conformers of the $CH_2$ bending vibration of the glycol group.[47] Compared to the original postconsumer PET sources (Figures 4ai,ii and S5a,b), the trans peak signals of their corresponding electrospun NF were relatively weak, while the gauche peaks appeared strengthened (Figures 4bi,ii and S5c,d).

Table S1 shows significant decreases in the T/G ratios for the 1340 and 1370 $cm^{-1}$ peaks ($T/G_{1340,\ 1370}$), as well as for the 972 and 1043 $cm^{-1}$ peaks ($T/G_{972,\ 1043}$). This indicates a significant decrease in the trans conformations in the electrospun PET NF compared to those in the original postconsumer PET sources. The crystalline region exclusively consists of the trans conformations, while the amorphous phase is primarily characterized by the presence of the gauche conformers.[48] Therefore, our FTIR data confirm the decreased %crystallinity observed in the DSC measurements of the electrospun PET NF, as shown in Table 1.

It is interesting to note that the electrospun PET NF samples showed a doublet band at 1261 and 1244 $cm^{-1}$ (Figure 4b), whereas the original postconsumer PET sources exhibited a single peak around 1240 $cm^{-1}$ (Figure 4a). This vibrational band splitting was attributed to crystal correlation field splitting, which typically occurs due to short-range interactions between closely packed molecules.[49,50] Considering the reduced presence of the crystalline region and the potential formation of the mesophase during electrospinning, the observed band splitting may be associated with the noncrystalline region of the PET chains. There are two conformational features of the noncrystalline PET with locally ordered structures: (1) an increased, isolated, and extended trans-rich conformation[33] and (2) an extended conformation consisting of kink conformers of the ethylene glycol fragment, with a ± gauche (—O−$CH_2$—) -trans (—$CH_2$—$CH_2$—) - ∓ gauche (—$CH_2$—O—) conformation.[20,34] Significant decreases in the T/G ratio were observed in the electrospun PET NF, as shown in Table S1. Therefore, it is more probable that the kink conformers have been formed in the noncrystalline regions, as suggested by modeling studies conducted by Auriemma et al.[51] The ethylene glycol bond conformations of gauche ± —O−$CH_2$—, trans —$CH_2$—$CH_2$—, and gauche∓ —$CH_2$—O— are known to have extended structures similar to those of the all-trans crystalline conformation.[20,34] An improved regularity achieved by the locally ordered structures in the noncrystalline region would contribute to more homogeneous polymer conformations in the local environments,[20] as supported by the improved FTIR resolution of the electrospun PET NF (Figures 3b).

**Crystallinity of Polyester-Textile NF and PET Bottle NF.** Figure 5 shows the XRD patterns acquired on the

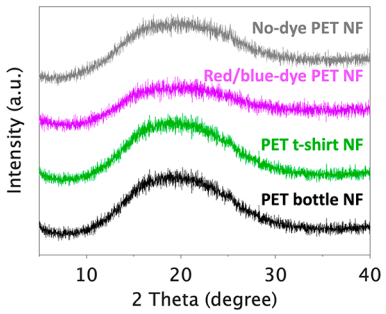


**Figure 5.** XRD patterns of the electrospun PET NF produced from the no-dye polyester fabric, the 50/50 mixture of red- and blue-dye polyester fabric, the polyester t-shirt, and the PET bottle.

electrospun NF from the no-dye polyester fabric, the 50/50 mixture of red- and blue-dye polyester fabric, the polyester t-shirt, and the PET bottle. No diffraction peaks were observed in any of the electrospun PET NF samples. Semicrystalline polyester fabrics typically exhibit characteristic peaks at 6.39°, 17.64°, 21.79°, 22.79°, and 26.12°[52] (JCPDS No. 4902301). The XRD data confirm that the electrospun NF obtained from the polyester textile sources and the PET bottle are predominantly amorphous. This observation is consistent with our FTIR data, which show attenuated intensities of the trans peaks but increased intensities of gauche peaks. Furthermore, this observation is confirmed by the decreased %crystallinity observed in the DSC results. Although XRD does not clearly detect the mesomorphic phase in PET, a skewed amorphous diffraction pattern provides evidence of its presence,[53] as previously noted by Strain et al.[6] This skewness was observed in Figure 5 for the electrospun NF produced from the postconsumer PET sources.

**Mechanical Properties of Polyester-Textile NF and PET Bottle NF.** Stress−strain curves and the Young's moduli of the electrospun NF produced from the no-dye polyester fabric, the 50/50 mixture of red- and blue-dye polyester fabric, the polyester t-shirt, and the PET bottle are shown in Figure 6. None of the samples ruptured at the end of the test, demonstrating the high flexibility of the electrospun PET NF. Distinct necking behavior was observed in the PET bottle NF, as evidenced by a plateau in tensile stress (Figure 6a). Similar behavior was also noted by Vedula et al., who highlighted that a region of alignment and orientation exists after the plateau region, resulting in strain-induced crystallization.[54] At the plateau region, PET chains that were not originally aligned become organized before breaking. In contrast, the electrospun NF produced from the polyester textile sources displayed a more rigid behavior prior to the breaking point (Figure 6a). The Young's moduli of the electrospun NF made from the polyester textile sources were approximately 2.5 times higher than that of the PET bottle NF, as shown in Figure 6b. Specifically, the values were 194.5 ± 10.8 MPa for the no-dye PET NF, 192.9 ± 7.5 MPa for the


https://doi.org/10.1021/acsapm.3c01232
ACS Appl. Polym. Mater. 2023, 5, 7298−7307

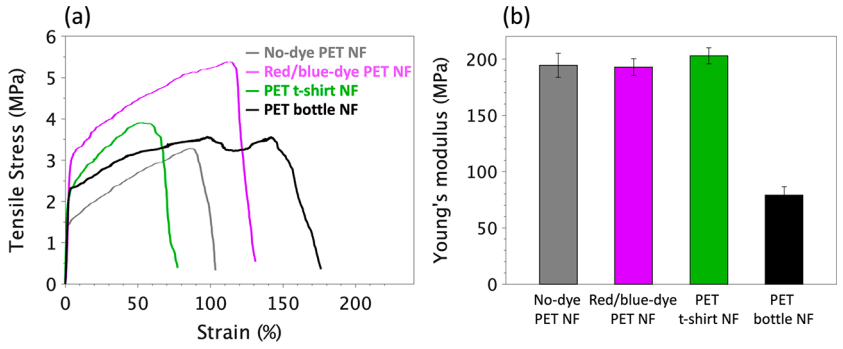


**Figure 6.** (a) Stress–strain curves and (b) Young's moduli of the electrospun NF produced from the no-dye polyester fabric, the 50/50 mixture of red- and blue-dye polyester fabric, the polyester t-shirt, and the PET bottle.

50/50 mixture of red- and blue-dye PET NF, 202.9 ± 7.2 MPa for the PET t-shirt NF, and 79.2 ± 7.4 MPa for the PET bottle NF. The higher Young's moduli observed in the polyester-textile NF can be attributed to a greater degree of molecular alignment present in the fibers with smaller diameters.[6,55]

**Thermal Degradation of Polyester-Textile NF and PET Bottle NF.** Figure 7 illustrates the TGA measurement of

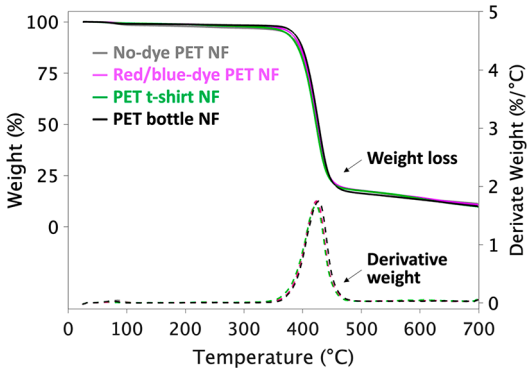


**Figure 7.** TGA results of the electrospun NF produced from the no-dye polyester fabric, the 50/50 mixture of red- and blue-dye polyester fabric, the polyester t-shirt, and the PET bottle.

the electrospun NF made from the no-dye polyester fabric, the 50/50 mixture of red- and blue-dye polyester fabric, the polyester t-shirt, and the PET bottle. A single-step degradation process, which is commonly observed for PET fibers,[5,56] appeared with a residue of approximately 10 wt %. The maximum decomposition temperatures of the polyester-textile NF and the PET bottle NF were 423 and 427 °C, which are within the reported ranges.[20,56,57] The similarity in the thermal degradation of all the electrospun PET NF indicates that there are no discernible differences in the chemical composition and thermal stability between those produced from the polyester textile sources and those from the PET bottle.

## CONCLUSIONS

In this study, we investigated the structural changes in electrospun nanofibers produced from several postconsumer polyester textile sources and a PET bottle. Our findings suggest that the changes are primarily attributed to the formation of the ordered structures in the noncrystalline region of the PET chains, as they undergo rapid stretching during electrospinning. All electrospun PET nanofibers exhibited lower degrees of crystallinity than those of their original postconsumer PET sources. The PET nanofibers produced from the postconsumer polyester textile sources exhibited notable distinctions compared to those from the PET bottle. Specifically, the nanofibers obtained from the polyester textile sources showed smaller average fiber diameters, higher degrees of crystallinity, higher melt-crystallization temperatures, and higher Young's moduli. The nanofibrous materials obtained from postconsumer PET textiles and bottles may hold promising potential for various applications such as filtration, protective clothing, and environmental uses.

## ASSOCIATED CONTENT

### Supporting Information

The Supporting Information is available free of charge at https://pubs.acs.org/doi/10.1021/acsapm.3c01232.

Digital photos of the original postconsumer PET sources; optical microscopy of the electrospun PET NF produced from the no-dye polyester fabric in a concentration of 20% (w/v) and of 24% (w/v); DSC curves of the as-spun PET t-shirt NF and the heat-set PET t-shirt NF; SEM image, fiber diameter distribution, and DSC curve of the TBAC-incorporated PET bottle NF; trans and gauche peak pairs of the FTIR spectra at 848 $cm^{-1}$, 898 $cm^{-1}$, 1471 $cm^{-1}$, and 1453 $cm^{-1}$, in the original postconsumer PET sources and their corresponding electrospun NF (PDF)

## AUTHOR INFORMATION

### Corresponding Author

**Tamer Uyar** – *Fiber Science Program, Department of Human Centered Design, College of Human Ecology, Cornell University, Ithaca, New York 14853, United States;* orcid.org/0000-0002-3989-4481; Email: tu46@cornell.edu

### Authors

**Yelin Ko** – *Fiber Science Program, Department of Human Centered Design, College of Human Ecology, Cornell University, Ithaca, New York 14853, United States*

**Juan P. Hinestroza** – *Fiber Science Program, Department of Human Centered Design, College of Human Ecology, Cornell University, Ithaca, New York 14853, United States*

Complete contact information is available at: https://pubs.acs.org/10.1021/acsapm.3c01232

### Author Contributions

YK: performed experiments, analyzed the data, and wrote the initial drafts. JPH: provided guidance on the data analysis, as well as reviewed and edited the manuscript. TU: provided initial planning of the experiments and guidance on the data analysis, as well as reviewed and edited the manuscript. The manuscript was written through the contributions of all authors. All authors have approved the final version of the manuscript.

### Notes

The authors declare no competing financial interest.

## ■ ACKNOWLEDGMENTS

This work made use of the Cornell Center for Materials Research Shared Facilities which are supported through the NSF MRSEC program (DMR-1719875), and Department of Human Centered Design Facilities. YK gratefully acknowledges financial support for this research by the Fulbright U.S. Student Program, which is sponsored by the U.S. Department of State and the Korean-American Educational Commission. Its contents are solely the responsibility of the author and do not necessarily represent the official views of the Fulbright Program, the Government of the United States, or the Korean-American Educational Commission.

## ■ REFERENCES

(1) U.S. Environmental Protection Agency. Advancing Sustainable Materials Management: 2018 Fact Sheet, 2020, https://www.epa.gov/sites/default/files/2021-01/documents/2018_ff_fact_sheet_dec_2020_fnl_508.pdf.

(2) S&P Global. *Chemical Economics Handbook - Polyester Fibers;* S&P Global: New York, 2022.

(3) Uyar, T.; Besenbacher, F. Electrospinning of Uniform Polystyrene Fibers: The Effect of Solvent Conductivity. *Polymer* **2008**, *49* (24), 5336−5343.

(4) Persano, L.; Camposeo, A.; Tekmen, C.; Pisignano, D. Industrial Upscaling of Electrospinning and Applications of Polymer Nanofibers: A Review. *Macromol. Mater. Eng.* **2013**, *298* (5), 504−520.

(5) Topuz, F.; Oldal, D. G.; Szekely, G. Valorization of Polyethylene Terephthalate (PET) Plastic Wastes as Nanofibrous Membranes for Oil Removal: Sustainable Solution for Plastic Waste and Oil Pollution. *Ind. Eng. Chem. Res.* **2022**, *61* (25), 9077−9086.

(6) Strain, I. N.; Wu, Q.; Pourrahimi, A. M.; Hedenqvist, M. S.; Olsson, R. T.; Andersson, R. L. Electrospinning of Recycled PET to Generate Tough Mesomorphic Fibre Membranes for Smoke Filtration. *J. Mater. Chem. A* **2015**, *3* (4), 1632−1640.

(7) Song, J.; Zhao, Q.; Meng, C.; Meng, J.; Chen, Z.; Li, J. Hierarchical Porous Recycled PET Nanofibers for High-Efficiency Aerosols and Virus Capturing. *ACS Appl. Mater. Interfaces* **2021**, *13* (41), 49380−49389.

(8) Hossain, M. T.; Shahid, M. A.; Ali, A. Development of Nanofibrous Membrane from Recycled Polyethylene Terephthalate Bottle by Electrospinning. *OpenNano* **2022**, *8*, No. 100089.

(9) Xiong, Q.; Tian, Q.; Yue, X.; Xu, J.; He, X.; Qiu, F.; Zhang, T. Superhydrophobic PET@ZnO Nanofibrous Membrane Extract from Waste Plastic for Efficient Water-In-Oil Emulsion Separation. *Ind. Eng. Chem. Res.* **2022**, *61* (32), 11804−11814.

(10) Roy, S.; Maji, P. K.; Goh, K. L. Sustainable Design of Flexible 3D Aerogel from Waste PET Bottle for Wastewater Treatment to Energy Harvesting Device. *Chem. Eng. J.* **2021**, *413*, No. 127409.

(11) Puguan, J. M. C.; Pornea, A. G. M.; Ruello, J. L. A.; Kim, H. Double-Porous PET Waste-Derived Nanofibrous Aerogel for Effective Broadband Acoustic Absorption and Transmission. *ACS Appl. Polym. Mater.* **2022**, *4* (4), 2626−2635.

(12) Chen, Y.; Zhao, B.; Zhang, H.; Zhang, T.; Yang, D.; Qiu, F. Laminated PET-Based Membranes with Sweat Transportation and Dual Thermal Insulation Properties. *Chem. Eng. J.* **2022**, *450*, No. 138177.

(13) Kongkhlang, T.; Tashiro, K.; Kotaki, M.; Chirachanchai, S. Electrospinning as a New Technique to Control the Crystal Morphology and Molecular Orientation of Polyoxymethylene Nanofibers. *J. Am. Chem. Soc.* **2008**, *130* (46), 15460−15466.

(14) Rieckmann, T.; Völker, S. Poly(Ethylene Terephthalate) Polymerization − Mechanism, Catalysis, Kinetics, Mass Transfer and Reactor Design. In *Modern Polyesters: Chemistry and Technology of Polyesters and Copolyesters;* John Wiley & Sons, 2005; pp 35−36.

(15) Kayaci, F.; Uyar, T. Electrospun Polyester/Cyclodextrin Nanofibers for Entrapment of Volatile Organic Compounds. *Polym. Eng. Sci.* **2014**, *54* (12), 2970−2978.

(16) Kayaci, F.; Aytac, Z.; Uyar, T. Surface Modification of Electrospun Polyester Nanofibers with Cyclodextrin Polymer for the Removal of Phenanthrene from Aqueous Solution. *J. Hazard. Mater.* **2013**, *261*, 286−294.

(17) Varma-Nair, M.; Wunderlich, B. Heat Capacity and Other Thermodynamic Properties of Linear Macromolecules X. Update of the ATHAS 1980 Data Bank. *J. Phys. Chem. Ref. Data* **1991**, *20* (2), 349−404.

(18) Boerio, F. J.; Bahl, S. K.; McGraw, G. E. Vibrational Analysis of Polyethylene Terephthalate and Its Deuterated Derivatives. *J. Polym. Sci., Polym. Phys. Ed.* **1976**, *14* (6), 1029−1046.

(19) Walls, D. J. Application of ATR-IR to the Analysis of Surface Structure and Orientation in Uniaxially Drawn Poly(ethylene terephthalate). *Appl. Spectrosc.* **1991**, *45* (7), 1193−1198.

(20) Bullions, T. A.; Wei, M.; Porbeni, F. E.; Gerber, M. J.; Peet, J.; Balik, M.; White, J. L.; Tonelli, A. E. Reorganization of the Structures, Morphologies, and Conformations of Bulk Polymers via Coalescence from Polymer-Cyclodextrin Inclusion Compounds. *J. Polym. Sci. B: Polym. Phys.* **2002**, *40* (10), 992−1012.

(21) Papkov, D.; Zou, Y.; Andalib, M. N.; Goponenko, A.; Cheng, S. Z. D.; Dzenis, Y. A. Simultaneously Strong and Tough Ultrafine Continuous Nanofibers. *ACS Nano* **2013**, *7* (4), 3324−3331.

(22) Ma, J.; Yu, L.; Chen, S.; Chen, W.; Wang, Y.; Guang, S.; Zhang, X.; Lu, W.; Wang, Y.; Bao, J. Structure-Property Evolution of Poly(ethylene terephthalate) Fibers in Industrialized Process under Complex Coupling of Stress and Temperature Field. *Macromolecules* **2019**, *52* (2), 565−574.

(23) Alves, N.M.; Mano, J.F.; Balaguer, E.; Meseguer Duenas, J.M.; Gomez Ribelles, J.L. Glass Transition and Structural Relaxation in Semi-Crystalline Poly(ethylene terephthalate): A DSC Study. *Polymer* **2002**, *43* (15), 4111−4122.

(24) Holdsworth, P. J.; Turner-Jones, A. The Melting Behaviour of Heat Crystallized Poly(ethylene terephthalate). *Polymer* **1971**, *12* (3), 195−208.

(25) Papkov, D.; Delpouve, N.; Delbreilh, L.; Araujo, S.; Stockdale, T.; Mamedov, S.; Maleckis, K.; Zou, Y.; Andalib, M. N.; Dargent, E.; Dravid, V. P.; Holt, M. V.; Pellerin, C.; Dzenis, Y. A. Quantifying Polymer Chain Orientation in Strong and Tough Nanofibers with Low Crystallinity: Toward Next Generation Nanostructured Superfibers. *ACS Nano* **2019**, *13* (5), 4893−4927.

(26) Soleimani, F.; Mazaheri, M.; Pellerin, C.; Bagheri, R. On the Importance of Noncrystalline Phases in Semicrystalline Electrospun Nanofibers. *ACS Appl. Polym. Mater.* **2021**, *3* (12), 6315−6325.

(27) Kim, J. S.; Lee, D. S. Thermal Properties of Electrospun Polyesters. *Polym. J.* **2000**, *32* (7), 616−618.

(28) Chen, K.; Zhang, W.; Yarin, A. L.; Pourdeyhimi, B. Polymer Melting Temperatures and Crystallinity at Different Pressure Applied. *J. Appl. Polym. Sci.* **2021**, *138* (37), No. 50936.

(29) Wang, C.; Lee, M. F.; Wu, Y. J. Solution-Electrospun Poly(ethylene terephthalate) Fibers: Processing and Characterization. *Macromolecules* **2012**, *45* (19), 7939−7947.

(30) Picciani, P. H. S.; Medeiros, E. S.; Pan, Z.; Orts, W. J.; Mattoso, L. H. C.; Soares, B. G. Development of Conducting Polyaniline/Poly(Lactic Acid) Nanofibers by Electrospinning. *J. Appl. Polym. Sci.* **2009**, *112* (2), 744−753.

(31) Cole, K. C.; Ajji, A.; Pellerin, E. New Insights into the Development of Ordered Structure in Poly(ethylene terephthalate). 1. Results from External Reflection Infrared Spectroscopy. *Macromolecules* **2002**, *35* (3), 770−784.
(32) Ma, Q.; Pyda, M.; Mao, B.; Cebe, P. Relationship Between the Rigid Amorphous Phase and Mesophase in Electrospun Fibers. *Polymer* **2013**, *54* (10), 2544−2554.
(33) Richard-Lacroix, M.; Pellerin, C. Orientation and Structure of Single Electrospun Nanofibers of Poly(ethylene terephthalate) by Confocal Raman Spectroscopy. *Macromolecules* **2012**, *45* (4), 1946−1953.
(34) Joijode, A. S.; Hawkins, K.; Tonelli, A. E. Improving Poly(ethylene terephthalate) Through Self-nucleation. *Macromol. Mater. Eng.* **2013**, *298* (11), 1190−1200.
(35) Stoclet, G.; Seguela, R.; Lefebvre, J. M.; Rochas, C. New Insights on the Strain-Induced Mesophase of Poly(d, l-Lactide): In Situ WAXS and DSC Study of the Thermo-Mechanical Stability. *Macromolecules* **2010**, *43* (17), 7228−7237.
(36) Chen, Y.; Han, L.; Ju, D.; Liu, T.; Dong, L. Disentanglement Induced by Uniaxial Pre-Stretching as a Key Factor for Toughening Poly(L-Lactic Acid) Sheets. *Polymer* **2018**, *140*, 47−55.
(37) Zuo, F.; Keum, J. K.; Chen, X.; Hsiao, B. S.; Chen, H.; Lai, S. Y.; Wevers, R.; Li, J. The Role of Interlamellar Chain Entanglement in Deformation-Induced Structure Changes During Uniaxial Stretching of Isotactic Polypropylene. *Polymer* **2007**, *48* (23), 6867−6880.
(38) Yang, Y.; Li, X.; Mi, J.; Ramakrishna, S.; Ji, D.; Yu, J.; Wang, R.; Qin, X. Coordinating Chain Crystallinity and Orientation by Tailoring Electrical Stretching for Fabrication of Super-Tough and Strong Organic Fibers. *Chem. Eng. J.* **2022**, *442*, No. 136203.
(39) Wang, C.; Fang, C. Y.; Wang, C. Y. Electrospun Poly(butylene terephthalate) Fibers: Entanglement Density Effect on Fiber Diameter and Fiber Nucleating Ability Towards Isotactic Polypropylene. *Polymer* **2015**, *72*, 21−29.
(40) Shenoy, S. L.; Bates, W. D.; Frisch, H. L.; Wnek, G. E. Role of Chain Entanglements on Fiber Formation During Electrospinning of Polymer Solutions: Good Solvent, Non-Specific Polymer-Polymer Interaction Limit. *Polymer* **2005**, *46* (10), 3372−3384.
(41) Lim, C. T.; Tan, E. P. S.; Ng, S. Y. Effects of Crystalline Morphology on the Tensile Properties of Electrospun Polymer Nanofibers. *Appl. Phys. Lett.* **2008**, *92* (14), 141908.
(42) Nguyen, N. Q.; Chen, T. F.; Lo, C. T. Confined Crystallization and Chain Conformational Change in Electrospun Poly(ethylene oxide) Nanofibers. *Polym. J.* **2021**, *53* (8), 895−905.
(43) Son, W. K.; Youk, J. H.; Lee, T. S.; Park, W. H. The Effects of Solution Properties and Polyelectrolyte on Electrospinning of Ultrafine Poly(ethylene oxide) Fibers. *Polymer* **2004**, *45* (9), 2959−2966.
(44) Fillon, B.; Wittmann, J. C.; Lotz, B.; Thierry, A. Self-Nucleation and Recrystallization of Isotactic Polypropylene ($\alpha$ Phase) Investigated by Differential Scanning Calorimetry. *J. Polym. Sci. B: Polym. Phys.* **1993**, *31* (10), 1383−1393.
(45) Sangroniz, L.; Cavallo, D.; Müller, A. J. Self-Nucleation Effects on Polymer Crystallization. *Macromolecules* **2020**, *53* (12), 4581−4604.
(46) Ajji, A.; Guevremont, J.; Cole, K. C.; Dumoulin, M. M. Orientation and Structure of Drawn Poly(ethylene terephthalate). *Polymer* **1996**, *37* (16), 3707−3714.
(47) Djebara, M.; Stoquert, J. P.; Abdesselam, M.; Muller, D.; Chami, A. C. FTIR Analysis of Polyethylene Terephthalate Irradiated by MeV $He^{+}$. *Nucl. Instrum. Methods Phys. Res. B* **2012**, *274*, 70−77.
(48) Manley, T. R.; Williams, D. A. Structure of Terephthalate Polymers I−Infra-red Spectra and Molecular Structure of Poly-(ethylene terephthalate). *Polymer* **1969**, *10*, 339−384.
(49) Koenig, J. L. *Spectroscopy of Polymers;* Elsevier, 1999.
(50) Lagaron, J. M.; Powell, A. K.; Davidson, N. S. Characterization of the Structure and Crystalline Polymorphism Present in Aliphatic Polyketones by Raman Spectroscopy. *Macromolecules* **2000**, *33* (3), 1030−1035.
(51) Auriemma, F.; Corradini, P.; Guerra, G.; Vacatello, M. Conformational Analysis of Highly Extended Poly(ethylene terephthalate) Chains by Monte Carlo Calculations. *Macromol. Theory Simul.* **1995**, *4* (1), 165−176.
(52) Zhao, Z.; Zhou, J.; Fan, T.; Li, L.; Liu, Z.; Liu, Y.; Lu, M. An Effective Surface Modification of Polyester Fabrics for Improving the Interfacial Deposition of Polypyrrole Layer. *Mater. Chem. Phys.* **2018**, *203*, 89−96.
(53) Keum, J. K.; Jeon, H. J.; Song, H. H.; Choi, J. I.; Son, Y. K. Orientation-Induced Crystallization of Poly(ethylene terephthalate) Fibers with Controlled Microstructure. *Polymer* **2008**, *49* (22), 4882−4888.
(54) Vedula, J.; Tonelli, A. E. Reorganization of Poly(ethylene terephthalate) Structures and Conformations to Alter Properties. *J. Polym. Sci. B: Polym. Phys.* **2007**, *45* (7), 735−746.
(55) Wang, C.; Lee, M. F.; Wu, Y. J. Solution-Electrospun Poly(ethylene terephthalate) Fibers: Processing and Characterization. *Macromolecules* **2012**, *45* (19), 7939−7947.
(56) Doan, H. N.; Phong Vo, P.; Hayashi, K.; Kinashi, K.; Sakai, W.; Tsutsumi, N. Recycled PET as a PDMS-Functionalized Electrospun Fibrous Membrane for Oil-Water Separation. *J. Environ. Chem. Eng.* **2020**, *8* (4), No. 103921.
(57) Kiani, S.; Mousavi, S. M.; Bidaki, A. Preparation of Polyethylene Terephthalate/Xanthan Nanofiltration Membranes Using Recycled Bottles for Removal of Diltiazem from Aqueous Solution. *J. Clean. Prod.* **2021**, *314*, No. 128082.


https://doi.org/10.1021/acsapm.3c01232
*ACS Appl. Polym. Mater.* 2023, 5, 7298−7307